Experimental/Computational Study of Viscous Flow in a Contracting Rectangular Elbow

J. C. Kreatsoulas,* D. Lee,† A. Ballantyne,* and C. J. Knight‡
Avco Research Laboratory, Inc., Everett, Massachusetts

Experimental results have been obtained for flow through a contracting, 90-deg, rectangular Stanitz elbow with thickened endwall boundary layers to generate passage vortices and strong secondary flow. This includes Pitot-static and LDV measurements for inflow boundary conditions. The data were used as the basis for three-dimensional viscous code validation based on a two-equation q-ω turbulence model using both integration to the wall and a wall-function treatment. Wall functions were found to be reliable for the complex three-dimensional flow considered. Eddy viscosity well away from walls appears to be overpredicted.

Introduction

THE Stanitz elbow was originally introduced to test certain aspects of secondary flow development in a turbine vane, namely, that associated with passage vortex formation and intensification in a contracting turn.[1] The geometry was designed to avoid adverse pressure gradients and hence the detrimental influence of separation. Experiments were conducted with the configuration shown in Fig. 1, including the option of spoilers upstream to simulate thickened endwall boundary layers which are characteristic of turbomachinery.[2] Subsequent studies on this rectangular duct at our organization will be the focus of this paper.

The experiment has been repeated to broaden the database, including wall pressure measurements on the endwall and operation at high subsonic Mach number. Definition of inflow boundary conditions is also emphasized due to significance of these in code validation. Computational studies assess modeling capability for a complex three-dimensional turbulent flowfield. This is based on Coakley's two-equation q-ω model,[3] using both integration to the wall and a wall-function treatment. The latter performs well even in the presence of strong secondary flow, and could lead to significant reduction in gridding requirements for three-dimensional viscous cascade flow simulation. Representative results from this combined experimental/theoretical study are summarized below.

Code Validation Experiment

The experiments were conducted in the Aerodynamic Test Facility[4] at Avco Research Laboratory (ARL). This facility can be operated in two modes: continuous operation at mass flow of up to 2.3 kg/s at 9.5 atm, or blowdown operation with mass flow up to 18 kg/s at 32 atm for 20 s test duration. The facility is fully computer controlled, including automated traversing equipment for Pitot-static and Pitot probes, and is capable of aggregate data-collection rates of 1 MHz into a MASSCOMP computer. This allows extensive data collection in a matter of seconds and display of results to assess data quality in minutes. Reliable and repeatable blowdown performance was established by conducting the Stanitz elbow experiment, an underlying reason for choosing a configuration that had been studied previously.

In the blowdown mode, LN_2 is pumped to 1800 psi, vaporized, and stored in a bottle bank. During blowdown the pressure inside the plenum, and therefore the mass flow rate through the test section, is maintained constant by a dome-loaded pressure regulator. A quick-acting butterfly valve is used for blowdown and flow shutoff. A 4×4 ft flow conditioner, with 1/8 in. hexagonal cell honeycomb and three screens, is used to reduce turbulence. The conditioner sidewalls are acoustically treated, with perforated baffles and acoustic foam, to reduce flow-generated noise. A 46:1 contraction is used for the transition to the test section.

A TSI model 9100-10 three-component, five-beam LDV system is also available. This was reconfigured for off-axis operation in a backscatter mode. Both the LDV and three-axis traverse system are controlled by an HP1000 computer, which also provides data analysis capability. Seed is provided via a pulsed-injection system, directing nominal 0.4-μm-diam TiO_2 particles into the flow-conditioning section only during LDV data acquisition, in order to minimize particle buildup on windows. LDV data were obtained with continuous mainstream flow.

The test section installed in the Aerodynamic Test Facility is a half-scale replica of the original Stanitz elbow. A photograph made during assembly was included in the original publication.[4] The short tunnel at the inlet and the extension at the exit of the elbow, illustrated in Fig. 1, have planar walls and are integrated with the elbow. In order to provide various thicknesses of incoming boundary layer on the plane walls of the elbow, spoilers were located at the junction between the last contraction and the tunnel. The spoilers were half-scale versions of those used by Stanitz, made out of 0.030-in. perforated sheet metal with 1/16-in.-diam holes, centered to form equilateral triangles, and spaced to give a ratio of metal area to total area of 0.6. Two spoiler sizes, projecting 1.91 and 3.18 cm into the airstream, were used in the tests. In addition, tests without spoilers were performed.

The test section was operated at elevated pressure in order to match Reynolds number, by constricting the flow downstream of the elbow. This allows independent control of exit Mach number and Reynolds number. The flat endwalls were reinforced by aluminum plates for such operation. Plenum chamber pressure and temperature and mass flow rate through an orifice plate provide the baseline flow data. Additional instrumentation includes 242 static pressure taps on the curved walls matched to locations used by Stanitz et al.,[2] 110 taps on one of the flat endwalls (where data were not obtained in the original experiment), exit plane total pressure surveys, and inlet plane Pitot-static surveys to determine boundary conditions. Thermally stabilized, autocalibrated SCANIVALVE

Presented as Paper 88-0186 at the AIAA 26th Aerospace Sciences Meeting, Reno, NV, Jan. 11-14, 1988; received Feb. 5, 1988; revision received Aug. 8, 1988.

*Principal Research Scientist. Member AIAA.
†Senior Research Scientist. Member AIAA.
‡Director, Engine Technology. Member AIAA.

ZOC-16 pressure transducers and pneumatic multiplexers are used for pressure measurements.

Inflow measurements deviate from the original experiment and will be discussed further here. Other experimental results will be given in conjunction with computational studies.

Pitot-static measurements of the inflow velocity profile in the ARL experiment are shown as solid lines in Fig. 2 for two upstream spoiler heights. These results are given in the spanwise direction, midway between pressure and suction surfaces, and were obtained with the elbow in place. The original Stanitz data are shown as discrete points. There is interference with the Pitot-static rake near the endwall, as is evident from the no-spoiler comparison. However, that does not explain the change in wake-region profile for the spoiled flow case. Independent LDV measurements also shown in Fig. 2 are in excellent agreement, lending strong support for the ARL profile. The normalized form is relatively insensitive to flow Mach number.

Two possible explanations for the discrepancy are noted. First, Stanitz et al.[2] made their entrance plane measurements with the elbow removed and using Pitot surveys. That precludes upstream influence of the elbow, which would most affect low-momentum fluid in the spoiler wake. Constant static pressure was also assumed in reducing the original data. That is definitely not true with the elbow in place. A second explanation for the profile change is that the spoiler effect may not have been duplicated in the half-scale experiment. However, we matched the spoiler configuration in terms of solidity as well as hole pattern and scaled hole diameter. Since global Reynolds number is matched, the latter should imply that hole Reynolds number is the same. Upstream displacement of spoilers is suitably scaled.

The inflow turbulence field is quite significant to code validation when a two-equation model is used, as will be made clear later. Root-mean-square velocity fluctuations were measured using the LDV in a two-component configuration, because the third component proved very noisy and unreliable. The data for both axial and vertical (between pressure and suction surfaces) components are shown in Fig. 3. There is noticeable anisotropy, and high turbulence intensity occurs over the spoiler wake region. Two theoretical curves are also shown in Fig. 3, both for isotropic turbulence. These are based on an equilibrium hypothesis to determine the turbulence parameter $\omega = \epsilon/k$, followed by matching eddy viscosity to an augmented Cebeci-Smith model to determine $q = k$. This is discussed in detail in the original publication.[4] The basic approach derives from Harsha and Lee.[5]

Computational Studies

Calculations are performed using a thin-layer Navier-Stokes code, known as DUCTAF,[6] which is based on scalar implicit approximate factorization, central differencing plus fourth-order damping, fully implicit boundary treatment, and a two-equation q-ω turbulence model. Both integration to the wall, using low-turbulence Reynolds number modeling, and a wall-function treatment are available,[4] the latter to relieve gridding requirements. Two primary issues were addressed in the computational studies. Code validation with properly defined inflow boundary conditions is one thrust. These were not available prior to the ARL experiment. The other important consideration is systematic evaluation of wall functions in the context of a complex three-dimensional internal flowfield involving strong secondary flow. Rather than trying to prove the existence of a logarithmic region in general, the approach is to assess the utility of such an assumption in situations representative of turbomachinery flow environments.

A basic issue in extending wall-function treatments to three dimensions is when flow turning ceases as the boundary is

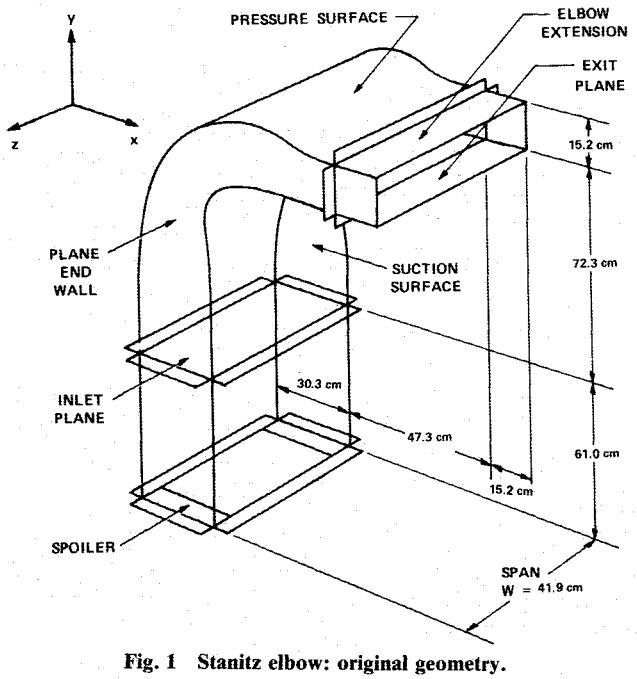

Fig. 1 Stanitz elbow: original geometry.

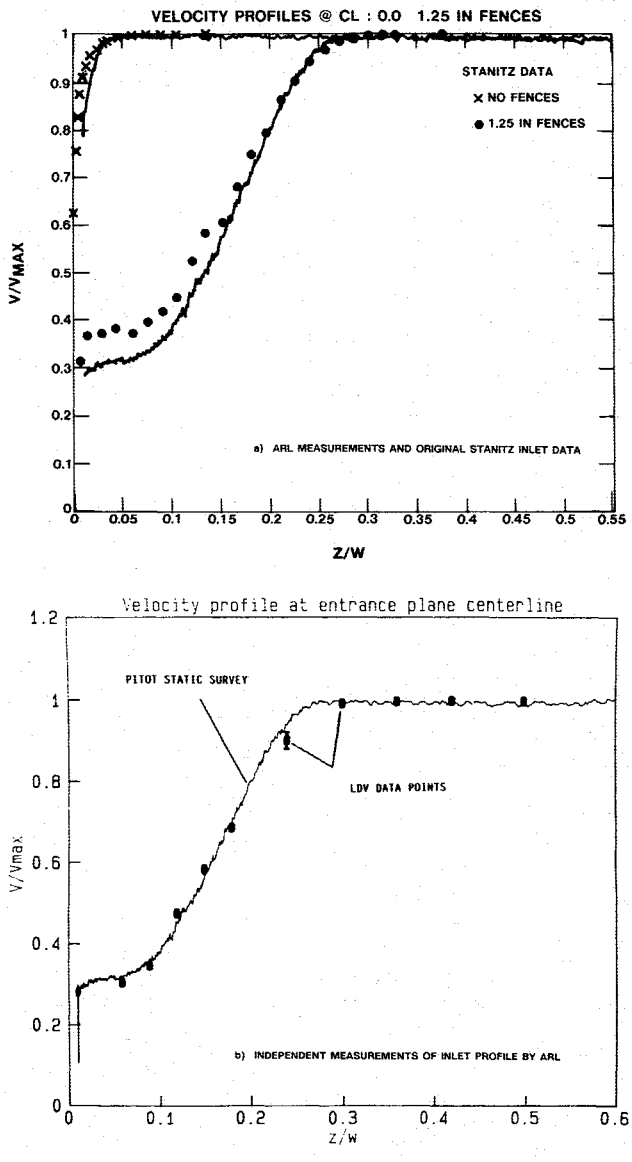

Fig. 2 Experimentally measured inflow velocity profiles.

approached, because such treatment implicitly assumes fixed flow angle between the wall and the first interior point. Theoretical work[7] indicates that there is generally a logarithmic region, with flow turning beginning for $y_+ > 40$–70 and primarily occurring in the defect layer. The treatment in the present study assumes that the limiting flow angle is achieved well outside the sublayer and is essentially constant for smaller values of y_+. Note that restrictions on y_+ at the first flux boundary arise in order for this to be assured. These are generally more stringent than for two-dimensional flows, and in consequence the gains for complex three-dimensional flowfields may not be as large.

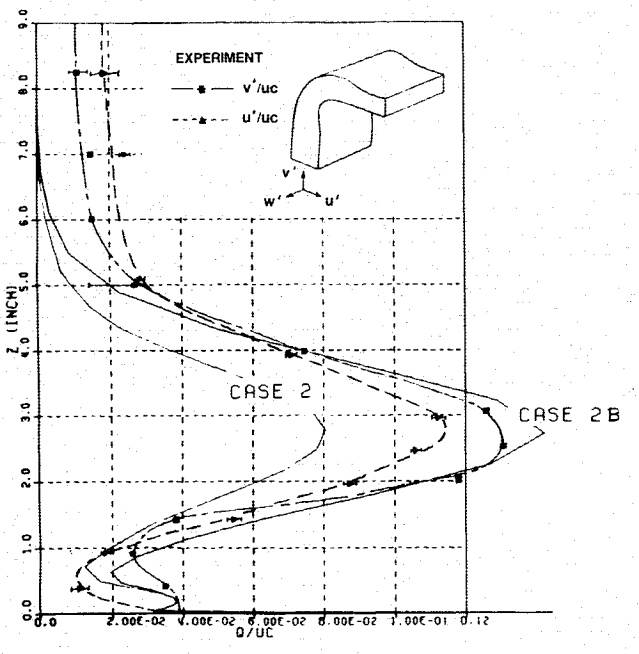

Fig. 3 Turbulence level at the elbow inflow plane.

Evaluation of the DUCTAF code was first done by comparison to the original experiment[2] for an isentropic exit Mach number $M_e = 0.4$ and reference Reynolds number $R_0 = 6.86 \times 10^5$, based on stagnation properties and a length of 2.54 cm. Only the 6.35-cm spoiler case was considered, and symmetry about midspan was assumed as established in the experiment. The transverse grid in each crossflow plane consisted of 38×27 points for integration to the wall (case 1) with a minimum spacing $\delta n_{\min}/H_i = 2.4 \times 10^{-4}$, where $H_i = 30.3$ cm is the inlet duct height in Fig. 1. This marginally resolves the viscous sublayer (with y_+ as large as 4 in some regions). With wall functions (case 2), the transverse gridding involved 30×20 points and the minimum spacing was increased by 50, so that the first cell is in the logarithmic region. In both cases, 27 axial grid points were used from the elbow inlet to the end of the 15.2-cm extension in Fig. 1. Note that the gain due to grid savings is $38 \times 27/30 \times 20 = 1.71$ with wall functions.

Stagnation pressure defect contours are compared at the exit of the straight 15.2-cm extension in Fig. 4, where $\Delta p_t = (p_{ti} - p_t)/(p_{ti} - p_e)$ is a total pressure loss coefficient, p_{ti} is the plenum pressure, p_e is the exit static pressure, and ϕ is the incompressible velocity potential used in defining the elbow geometry.[1] Exit Mach number and reference Reynolds number were matched to the experiment. Note that the contour pattern in computational results is essentially unaffected by wall boundary treatment. There are notable discrepancies from experiment. This includes the degree of evolution of the $\Delta p_t = 0.05$ contour at midspan and differences in detail for the $\Delta p_t = 0.25$ and 0.30 contours. Note also that there is some question about the experimental measurement of the $\Delta p_t = 0.05$ contour in the endwall/suction surface quadrant, especially when compared to ARL experimental results discussed later.

Variation of the mass-average Δp_t is shown in Fig. 5 vs the axial coordinate ϕ, defined above. Data points at the elbow inlet and at the end of the straight extension are from the original experiment. Much better agreement is achieved with wall functions (0.5 vs 11%), without any parameter adjustment. Inaccurate τ_w evidently arises in case 1, indicating the need to reduce the minimum grid spacing for integration to the

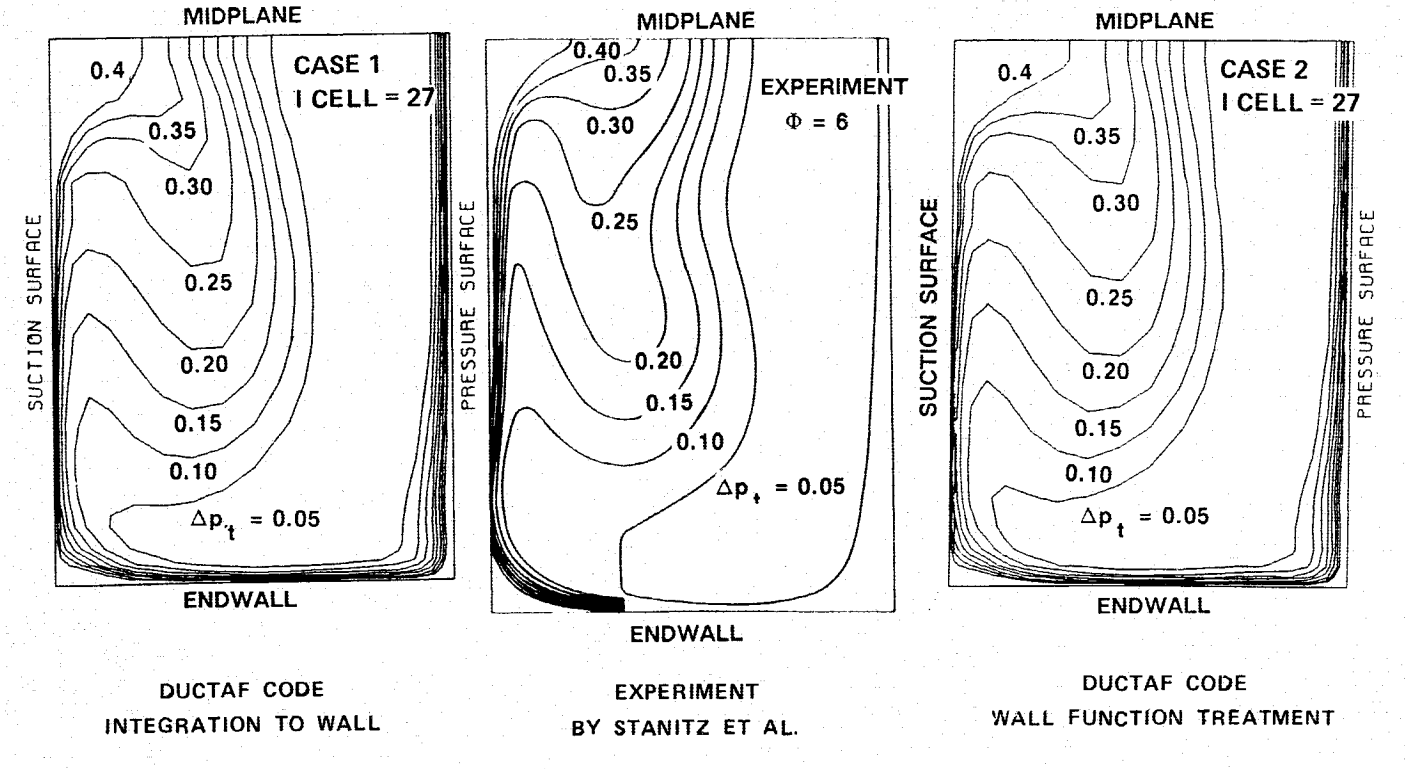

Fig. 4 Comparison of predicted Δp_t contours at $\phi = 6$ to experiment.

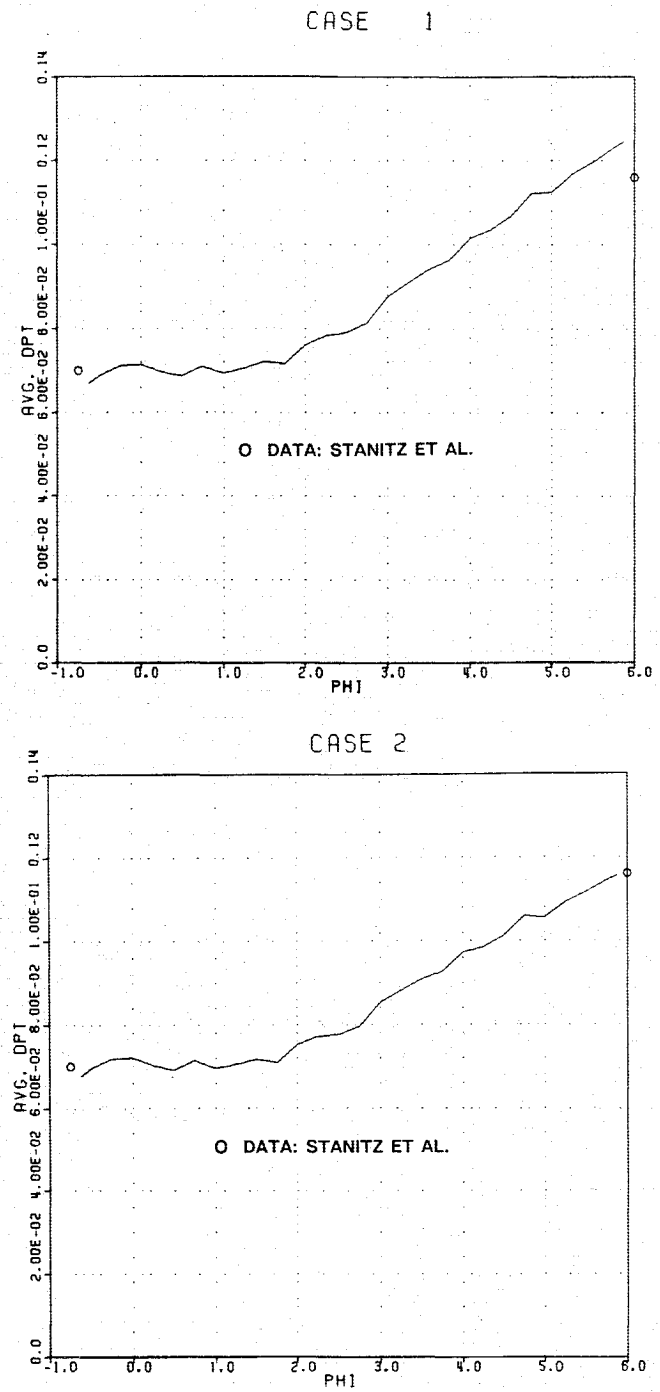

Fig. 5 Axial variation of mass-average pressure loss using two wall-boundary treatments.

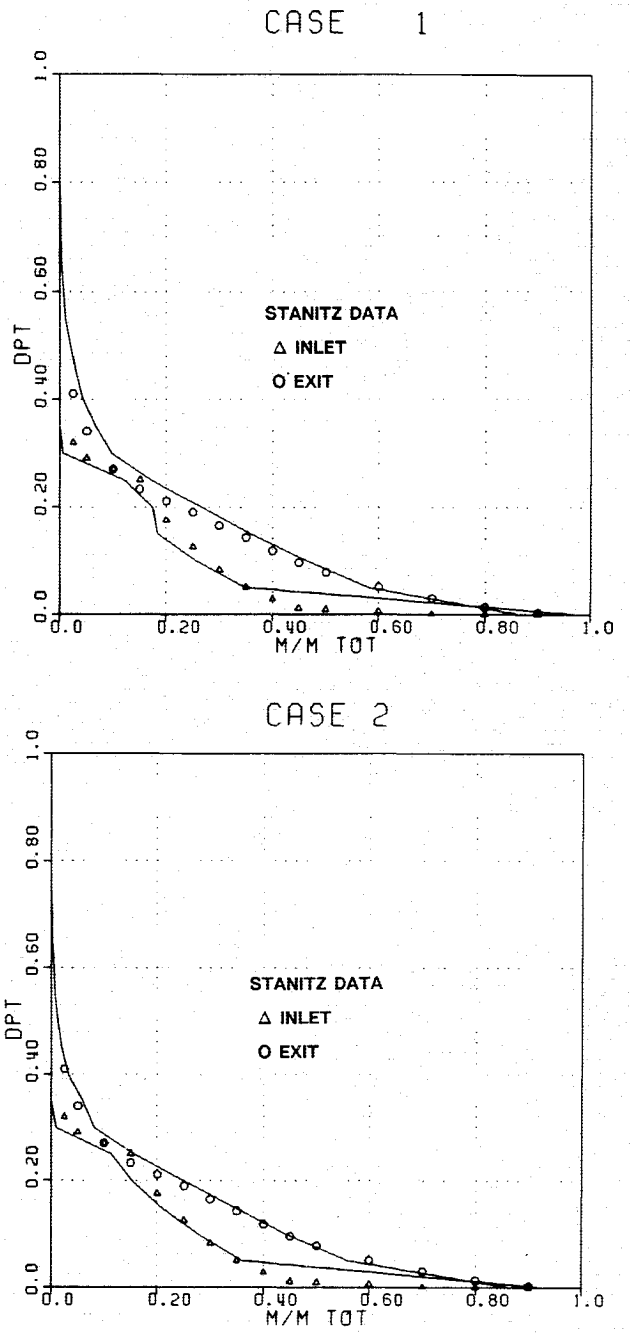

Fig. 6 Variation of inlet and exit Δp_t with mass-flow fraction, using two wall-boundary treatments.

wall and adjust turbulence constants to values appropriate to $y_+ \leq 1$. Improved means of incorporating turbulence source terms in the implicit update procedure[8] would presumably make this straightforward. The treatment of source terms now in DUCTAF is basically the same as that originally suggested by Coakley.[3]

A useful way to evaluate the accuracy of the algorithm in terms of stagnation pressure transport is to plot Δp_t as a function of the mass-flow fraction m/m_{total}, as shown in Fig. 6. At the exit plane, both integration to the wall and the wall-function treatment show good agreement with experiment. Case 2 results are somewhat better because frictional losses are more accurately predicted. At the inlet plane, both solutions show poor agreement near $m/m_{\text{total}} = 0.15$, with the sharp drop in DUCTAF results due to the coarse inviscid-core grid. It was possible to reduce this by refining the grid to better resolve the inlet spoiler wake profile, but the overall effect was found not significant. Discrepancy at the inlet for small values of Δp_t is almost assuredly due to using excessively large bins in constructing the plot because the assumed inlet velocity profile is uniform beyond a quarter-span, outside the spoiler wake.

A further check on the wall-function treatment is provided by considering the near-wall flow direction. Unit vectors for cases 1 and 2 are shown in Fig. 7 to schematically display results with the two boundary treatments. with the suction surface below, pressure surface above, and endwall between. Use of unit vectors avoids the fact that velocity magnitude at the first cell is substantially different for these cases. As can be seen, the flow pattern is essentially unchanged between the two boundary treatments. Thus, negligible flow turning occurs near the wall, as assumed in applying wall functions. If the same holds true for cascades, especially near the horseshoe vortex where flow is considerably less benign, there should be

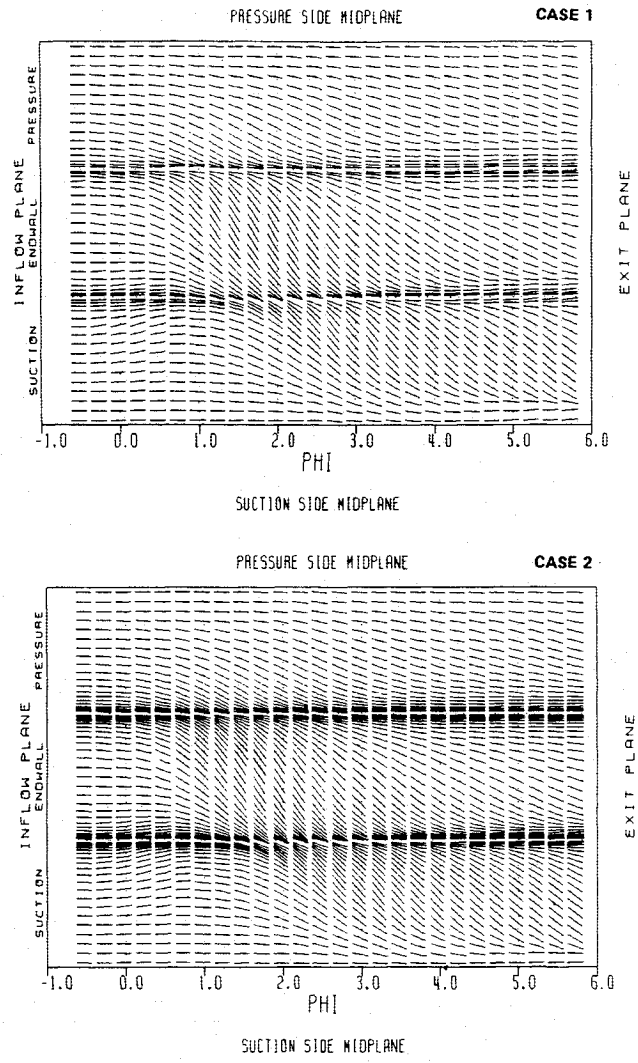

Fig. 7 Schematic display of near-wall flow directions.

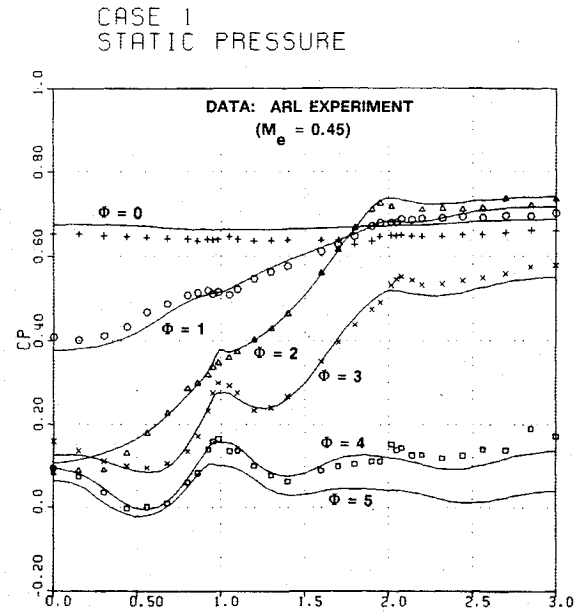

Fig. 8 Comparison of predicted wall pressure to ARL experiment.

little question about applicability of wall functions to complex three-dimensional flowfields in turbomachinery.

Wall static pressure was measured on the endwall in the ARL experiment to permit more complete code validation. The experiment involved $M_e = 0.45$ and $R_0 = 5.93 \times 10^5$. Data and code results are plotted around the duct periphery at selected axial stations in Fig. 8, with suction surface results for abscissa values between zero and one, endwall results between one and two, and pressure surface results between two and three. Note that $C_p = (p - p_e)/(p_{ti} - p_e)$, where p_e is the exit static pressure and p_{ti} is the plenum pressure. Computational results are only shown for integration to the wall because wall functions gave almost indistinguishable predictions.[4] Pressure is evidently near its exit value at the beginning of the straight extension ($\phi = 5$). There is a jump in experimental data for $\phi = 4$ at the endwall/pressure surface juncture. This is due to a shift upstream of probe-hole location during elbow fabrication; i.e., the data are not exactly at $\phi = 4$ on the pressure surface. Computational results for C_p were obtained for $M_e = 0.40$, slightly lower than experimental conditions at $M_e = 0.45$. Nevertheless, agreement is consistently good and essentially independent of wall-boundary treatment. Calculations with $M_e = 0.45$ showed improvement mainly for $\phi = 0$.

Pitot measurements at ARL were done before the straight extension section, at $\phi = 5$, in contrast to the original Stanitz experiment. These are shown in Fig. 9, along with computational results. Comparison to the experimental contour in Fig. 4 indicates reasonable agreement between experiments, consistent with expected evolution over $5 \leq \phi \leq 6$ and experimental error. Code results in Fig. 9 using the two wall-boundary treatments are almost indistinguishable from each other, but exhibit notable discrepancy from experiment near midplane. This was also evident in Fig. 4. Recognize that the original inflow velocity profile was used in these computational studies. The effect of using the ARL inflow profile, which is different, will be addressed below. There is another interesting feature in Fig. 9. The ARL data indicate a corner vortex at the endwall/suction surface juncture, conceivably due to anisotropic turbulence effects. This was not evident in the original measurements.

Results in Fig. 10 indicate the effect of inflow velocity profile. Integration to the wall is used with the original profile and $M_e = 0.4$ for case 1, and with the ARL profile and $M_e = 0.45$ for case 1M. Inflow turbulence, based on the case 2 profile in Fig. 3, is well below the experimental estimate. Greater wake defect at the inflow plane plus larger M_e lead to more secondary flow and better agreement of the $\Delta p_t = 0.05$ contour with experiment at midspan. The peak secondary flow speed is 0.162 for case 1 and 0.178 for case 1M, normalized by the stagnation sound speed. There is noticeable deviation of $\Delta p_t = 0.2$ and 0.3 contours from experiment at midspan. It would be relevant to incorporate streamline curvature effects into the q-ω model to assess impact. That could also alter the turbulent eddy viscosity in the middle of the elbow, where the passage vortex tends to remain for the large spoiler height considered.

Code results in Fig. 11 show marked influence of the inlet turbulence intensity profile, defined for the two cases in Fig. 3. This persistent effect arises because the wake exhibits high turbulence level and has substantial dimension, limiting natural decay and the effect of flow contraction. Several processes appear to be involved. First, enhanced turbulence would tend to smooth features in the stagnation pressure distribution due to diffusion. Somewhat increased viscous loss for case 2B implies augmented Reynolds stresses, as expected with higher turbulence intensity. That can in turn retard secondary flow due to drag. It is also likely that enhanced mixing could reduce the wake-momentum defect and hence centrifugal force differential within the turn. Although not shown, the pattern of secondary flow is not much affected, just the magnitude. The peak secondary flow is 0.165 for case 2 and 0.141 for case 2B, both at $\phi = 3.3$ as for Fig. 10.

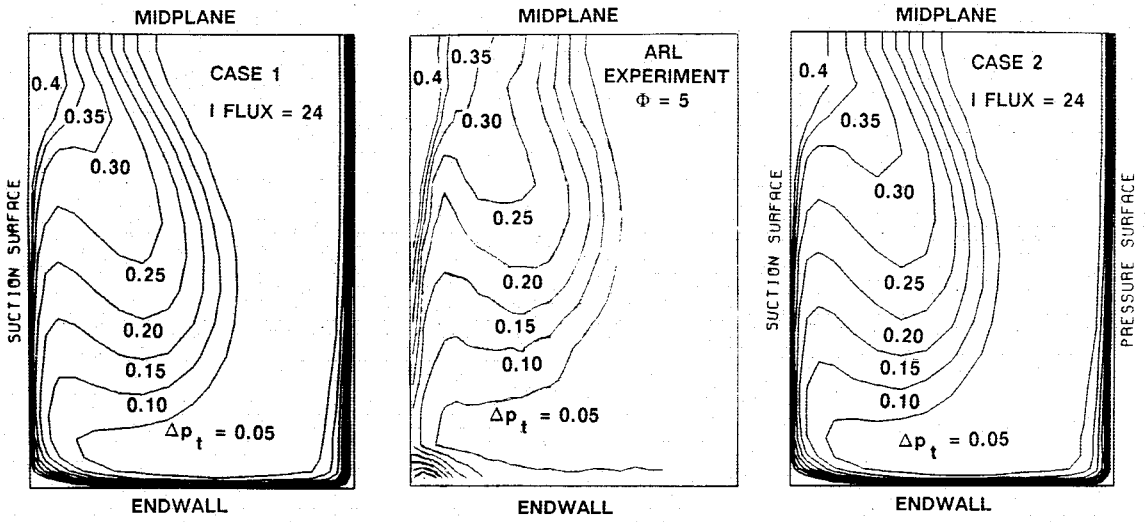

Fig. 9 Comparison of DUCTAF results with measured Δp_t at $\phi = 5$.

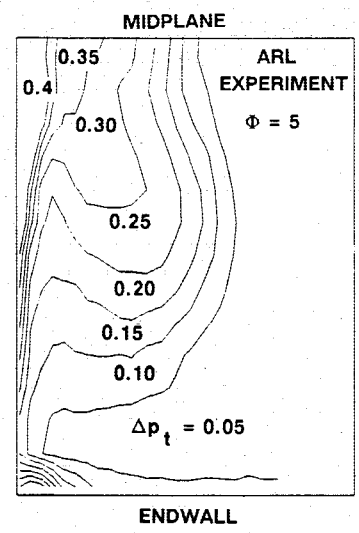

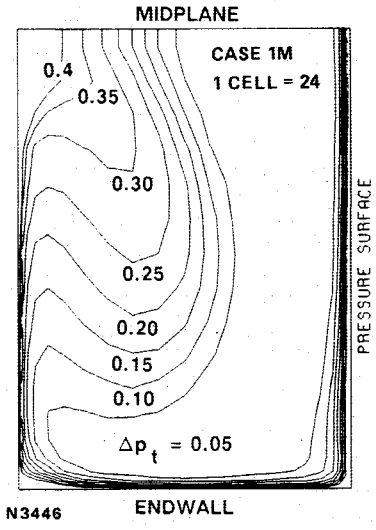

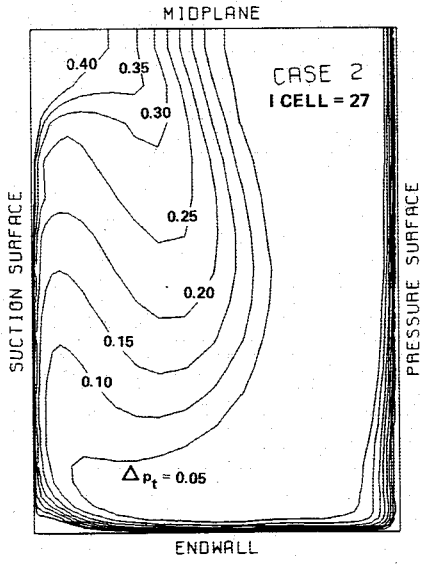

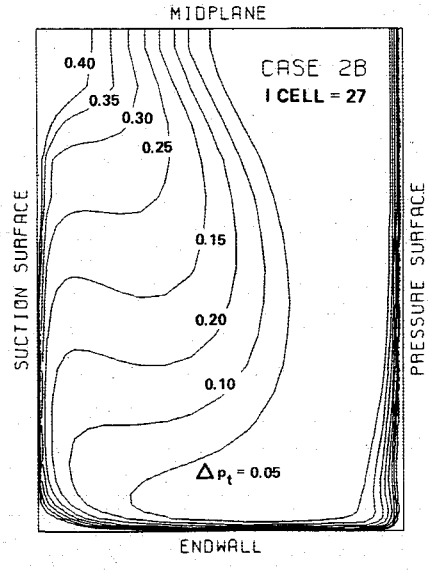

Fig. 10 Effect of altered inflow velocity profile on Δp_t at $\phi = 5$.

Fig. 11 Effect of inflow turbulence on flow predictions at $\phi = 6$.

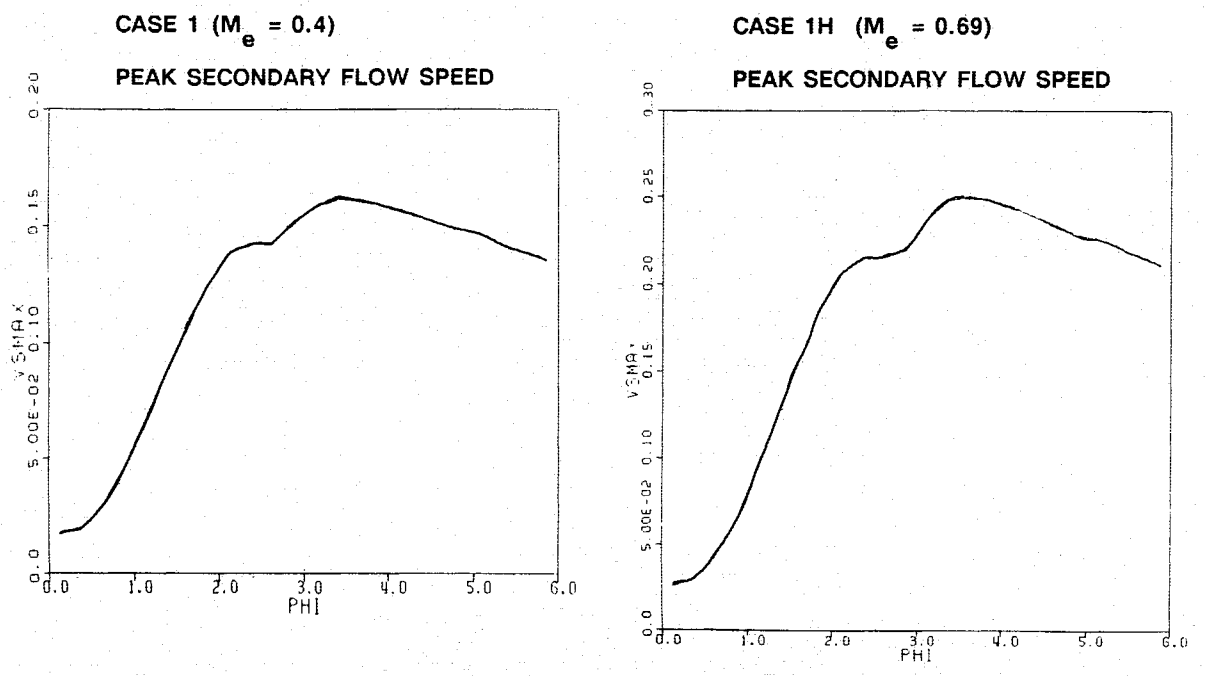

Fig. 12 Comparison of secondary flow evolution for two exit Mach numbers.

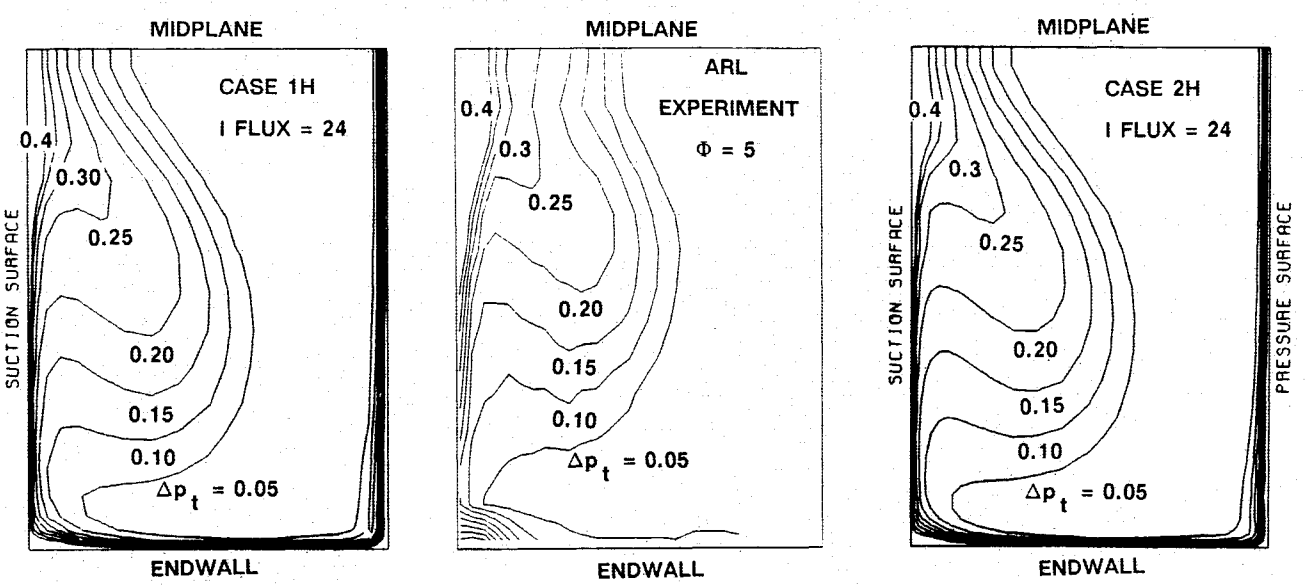

Fig. 13 Comparison of DUCTAF results with measured Δp_t at $\phi = 5$ for $M_e = 0.69$.

Comparing Fig. 10 and 11, the measured inflow velocity and turbulence profiles have contrary influences on baseline behavior. Putting both together will not lead to good agreement with experiment. There is a strong tendency to conclude that there may be a fundamental issue with the current turbulence modeling: eddy viscosity in the core region seems too high. This could be due to absence of an intermittency factor in standard two-equation models, or streamline curvature effects (including that due to swirl) could be needed.

Code performance was also assessed at high subsonic Mach number, $M_e = 0.69$, using the two wall-boundary treatments: integration to the wall (case 1H) and wall functions (case 2H). The reference Reynolds number $R_0 = 4.36 \times 10^5$, as in the corresponding ARL experiment. Gridding was the same as at lower Mach number, and minimum grid spacing increased by a factor of 50 with wall functions.

The peak secondary flow speed is increased only moderately at higher Mach number, as can be seen by comparing results in Fig. 12 for $M_e = 0.4$ and $M_e = 0.69$. Essentially the same curves are obtained with wall functions. Since centrifugal force scales as M^2 and transit time as $1/M$, where M is a representative mean Mach number, secondary velocity should scale linearly with M. Quasi-one-dimensional relations give inlet $M_i = 0.205$ and 0.275, respectively, and $M \sim (M_i + M_e)/2$ is reasonable. Figure 12 shows roughly a 50% increase in secondary flow at the higher M_e, as expected. Note that this same scaling argument can be extended to conclude that low-momentum fluid displacement should be insensitive to Mach number. That is consistent with experimental observations to first order.

Predicted loss contours for $M_e = 0.69$ are compared to ARL experiment at $\phi = 5$ in Fig. 13, showing again some discrepancy at midplane. Reference to Figs. 4 and 9 and associated discussion is relevant. DUCTAF results are similar for either wall-boundary treatment. This is taken as a strong indication that there should be no issue in utilizing a wall-

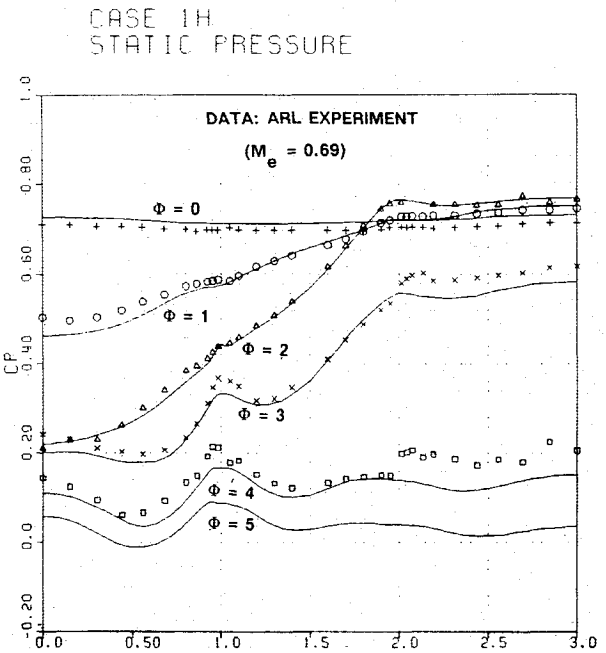

Fig. 14 Predicted wall pressure compared to experiment at $M_e = 0.69$.

function treatment for three-dimensional transonic cascade flowfields. As before, there is some indication of a corner vortex in the ARL experiment. Predicted wall static pressure contours shown in Fig. 14 are also in reasonable agreement with experiment. Again, only results for integration to the wall are shown because those obtained using wall functions are almost indistinguishable.[4]

Conclusion

Based on a detailed experimental study and a computational study comparing the wall-function boundary treatment with integration to the wall and both results to experiments, the following conclusions have been reached:

1) High-quality data, suitable for code validation purposes, were obtained using a blowdown mode of operation. The agreement with the original steady-state experiment is good, providing support for the reliability of data collection with intermittent operation in the Aerodynamic Test Facility. The quality of the data was further confirmed by limited LDV measurements under continuous flow conditions.

2) The ARL experimental data set includes information not previously available for the Stanitz elbow. This includes complete three-dimensional inlet plane velocity contours, inflow turbulence quantities needed to assess two-equation modeling, endwall static pressure measurements, and study of compressibility effects over the exit Mach number range $M_e = 0.4$–0.69.

3) The wall-function boundary treatment gives reliable results, with secondary flow and loss contours in crossflow planes essentially indistinguishable from those for integration to the wall. Mass-average loss prediction is significantly improved due to more accurate wall shear stress using wall functions. This is due to inadequacies in DUCTAF which dictated minimum grid spacing that is too large to adequately resolve the viscous sublayer. Handling of turbulence source terms has recently been improved in a viscous cascade code.[8]

4) Relative to the original results, secondary flow increases when the ARL inflow velocity profile is used with turbulence level unchanged, and decreases when the inflow turbulence is increased to the level estimated from LDV measurements at ARL with the velocity profile unchanged. The former moves exit Δp_t contours into better agreement with experiment, whereas the latter does the opposite.

5) A plausible conclusion based on these observations is that the eddy viscosity is being overestimated in the central core region with the current turbulence formulation. This might be remedied by incorporating streamline curvature effects into the turbulence modeling, including that associated with swirl flow. Intermittency effects might also have a moderating influence. Further experimental study is relevant to support and guide such modeling efforts.

6) The number of grid points can be significantly reduced using wall functions. Also, convergence rate is considerably enhanced in DUCTAF compared with integration to the wall. It is not clear to what extent the latter would apply with improved turbulence source-term treatment. These two contributing factors provide much improved computational economy in the wall-function version of DUCTAF.

Acknowledgment

This research was conducted under the sponsorship of Textron Lycoming's Research and Development Program. The authors wish to thank the Textron Lycoming management for their support and permission to present these results.

References

[1]Stanitz, J. D., "Aerodynamic Design of Efficient Two-Dimensional Channels," *Transactions of the American Society of Mechanical Engineers,* Vol. 75, Oct. 1953, pp. 1241–1256.

[2]Stanitz, J. D., Osborn, W. M., and Mizisin, S., "An Experimental Investigation of Secondary Flow in an Accelerating, Rectangular Elbow with 90° of Turning," NACA 3015, 1953.

[3]Coakley, T. J., "Turbulence Modeling Methods for the Compressible Navier-Stokes Equations," AIAA Paper 83-1693, June 1983.

[4]Kreatsoulas, J. C., Lee, D., Ballantyne, A., and Knight, C. J., "Experimental/Computational Study of Viscous Flow in an Accelerating, 90-Degree, Rectangular Elbow," AIAA Paper 88-0186, Jan. 1988.

[5]Harsha, P. T. and Lee, S. C., "Correlation Between Turbulent Shear Stress and Turbulent Kinetic Energy," *AIAA Journal,* Vol. 8, Aug. 1970, pp. 1508–1510.

[6]Knight, C. J. and Bozzola, R., "Implicit Time-Asymptotic Treatment of Subsonic 3D Viscous Flow in Duct Geometries," AIAA Paper 85-1627, July 1985.

[7]Goldberg, U. and Reshotko, E., "Scaling and Modeling of Three-Dimensional, Pressure Driven, Turbulent Boundary Layers," AIAA Paper 83-1695, July 1983.

[8]Knight, C. J. and Choi, D., "Development of a Viscous Cascade Code Based on Scalar Implicit Factorization," AIAA Paper 87-2150, June 1987.